

Published in final edited form as:

Immunity. 2013 October 17; 39(4): . doi:10.1016/j.immuni.2013.09.006.

Granulocyte Macrophage-Colony Stimulating Factor-induced Zn Sequestration Enhances Macrophage Superoxide and Limits Intracellular Pathogen Survival

Kavitha Subramanian Vignesh^{1,2,†}, Julio A. Landero Figueroa^{3,†}, Aleksey Porollo⁴, Joseph A. Caruso³, and George S. Deepe Jr^{2,5,*}

¹Department of Molecular Genetics, Biochemistry, Microbiology and Immunology, University of Cincinnati, OH 45267 USA

²Division of Infectious Diseases, College of Medicine, University of Cincinnati, Cincinnati, OH 45267 USA

³University of Cincinnati/Agilent Technologies Metallomics Center of the Americas, Department of Chemistry, University of Cincinnati, Cincinnati, OH 45221 USA

⁴Department of Environmental Health, University of Cincinnati, Cincinnati, OH 45267 USA

⁵Veterans Affairs Hospital, Cincinnati, OH 45220 USA

SUMMARY

Macrophages possess numerous mechanisms to combat microbial invasion, including sequestration of essential nutrients, like Zn. The pleiotropic cytokine granulocyte macrophage-colony stimulating factor (GM-CSF) enhances antimicrobial defenses against intracellular pathogens such as *Histoplasma capsulatum*, but its mode of action remains elusive. We have found that GM-CSF activated infected macrophages sequestered labile Zn by inducing binding to metallothioneins (MTs) in a STAT3 and STAT5 transcription factor-dependent manner. GM-CSF upregulated expression of Zn exporters, *Slc30a4* and *Slc30a7* and the metal was shuttled away from phagosomes and into the Golgi apparatus. This distinctive Zn sequestration strategy elevated phagosomal H⁺ channel function and triggered reactive oxygen species (ROS) generation by NADPH oxidase. Consequently, *H. capsulatum* was selectively deprived of Zn, thereby halting replication and fostering fungal clearance. GM-CSF mediated Zn sequestration via MTs *in vitro* and *in vivo* in mice and in human macrophages. These findings illuminate a GM-CSF-induced Zn-sequestration network that drives phagocyte antimicrobial effector function.

Contact: George S. Deepe, Jr. MD, george.deepe@uc.edu, Phone-513-558-4706, Fax-513-558-2089.

[†]These authors contributed equally to this work.

COMPETING FINANCIAL INTERESTS

The authors declare no competing financial interests.

Publisher's Disclaimer: This is a PDF file of an unedited manuscript that has been accepted for publication. As a service to our customers we are providing this early version of the manuscript. The manuscript will undergo copyediting, typesetting, and review of the resulting proof before it is published in its final citable form. Please note that during the production process errors may be discovered which could affect the content, and all legal disclaimers that apply to the journal pertain.

K.S.V and J.L.F. contributed equally, designed and performed experiments, analyzed data and wrote the manuscript, K.S.V performed *in vitro*, microscopy, *in vivo* and human experiments and interpreted data, J.L.F. performed chromatographic separations with UV-Vis, ICP-MS and ESI-IT-MS-MS analysis and interpreted data, A.P. performed bioinformatics analysis, J.C. and G.S.D. designed and supervised the work. All authors participated in final manuscript preparation.

INTRODUCTION

Zn is an abundant transition metal in living organisms. It is essential in immune homeostasis and function and Zn deficiency has been associated with thymic atrophy, impaired B, T and NK cell responses and T helper-1 (Th1) cytokine production (Fraker et al., 1986). Zn also functions in intracellular signaling (Hirano et al., 2008). Such a wide association with cellular functions requires strict regulation of Zn.

Availability of Zn to biomolecules is tightly regulated by binding proteins, metallothioneins (MTs) and Zn transporters. MTs are cysteine-rich proteins that bind up to seven Zn ions with picomolar affinity and carry the labile Zn fraction to cellular compartments. MTs are induced during oxidative stress, scavenge reactive oxygen species (ROS) and reduce heavy metal intoxication (Coyle et al., 2002).

Macrophages are crucial role in immune defense; they phagocytose and kill intracellular pathogens by oxidative burst, nitric oxide production (Fang, 1997) and T cell activation (Mosser, 2003). 'Nutritional immunity' signifies deprivation of essential nutrients to pathogens, thereby exerting an antimicrobial effect (Appelberg, 2006). In this regard, interferon gamma (IFN- γ) deprives Fe in macrophages by regulating transferrin receptors and the transporter *Slc11a1* (Nairz et al., 2008; Zwillig et al., 1999). In contrast, macrophages may intoxicate *Mycobacterium tuberculosis* with Zn in phagosomes (Botella et al., 2011). Zn competitively inhibits Mn binding to an essential virulence determinant in *Streptococcus pneumoniae* (McDevitt et al., 2011), rendering it inactive. Thus, both metal starvation and intoxication are part of the arsenal employed by macrophages in host defenses.

Apart from directly exploiting metals for combating pathogens, immune cells also need them for activation of defense mechanisms. In this regard, modulation of Zn activates microglia (Kauppinen et al., 2008) and dendritic cells (Kitamura et al., 2006) by altering surface markers and cytokine expression. Thus, Zn regulation is crucial in determining the outcome of an infectious process.

The fungal pathogen, *H. capsulatum*, is distributed worldwide and causes pulmonary and disseminated histoplasmosis, particularly in immunocompromised patients. For clearance of infection, coordinated action of innate and adaptive immunity is essential. The fungus gains entry into the host primarily via pulmonary route, is phagocytosed and replicates within resting macrophages (Howard, 1964). Activation of macrophages with IFN- γ or GM-CSF promotes fungal growth inhibition. While IFN- γ acts only on murine macrophages *in vitro*, GM-CSF inhibits growth of yeasts in both murine and human macrophages (Newman and Gootee, 1992). A lack of GM-CSF is lethal during infection and treatment with recombinant GM-CSF accelerates fungal clearance (Deepe et al., 1999).

We have reported that Zn is essential for survival of *H. capsulatum* within macrophages and chelation causes drastic retardation of fungal growth. (Winters et al., 2010). Here, we elucidate a mechanism by which GM-CSF activates macrophages to preferentially sequester Zn while enhancing ROS production and denying the intracellular pathogen, access to this element. Using a murine pulmonary model of *H. capsulatum* infection *in vivo*, we reveal the significance of GM-CSF in Zn sequestration by MTs in infected macrophages. Finally, we have shown that this effect of GM-CSF is conserved in human macrophages.

RESULTS

GM-CSF modulates total Zn and Zn proteome distribution

An unbiased inductively coupled plasma-mass spectrometry (ICP-MS) total elemental analysis was performed to evaluate changes in the concentration of Zn, Fe, Cu and Mn in macrophage lysates and *H. capsulatum* itself. The total Zn concentration increased in GM-CSF activated peritoneal macrophages compared to the resting control, and increased further in activated peritoneal and bone marrow macrophages during infection with 5 yeasts per macrophage. In contrast, Zn concentration was significantly reduced ($p < 0.001$) in *H. capsulatum* recovered from activated macrophages in comparison to yeasts from resting peritoneal macrophages, and media-cultured *H. capsulatum*, suggesting that GM-CSF activation induced deprivation of yeast associated Zn. GM-CSF also altered Fe within macrophages, but not in intracellular yeasts. Meanwhile, activation did not alter the concentration of Cu and Mn in macrophages and yeasts (Figures 1A and 1B). Thus, GM-CSF specifically altered Zn flux in *H. capsulatum* infected peritoneal and bone marrow macrophages.

To examine the Zn-proteome distribution in macrophages, we used size exclusion chromatography based on molecular size via hydrodynamic radii coupled to ICP-MS (SEC-ICP-MS). The Zn signal increased upon exposure to GM-CSF compared to resting peritoneal macrophages and a greater increase was seen upon activation and infection (Figure 1C). A large increment in the Zn signal was observed in infected activated bone marrow macrophages compared to uninfected control (Figure 1D). The relative Zn distribution between fractions was altered; the principal change occurred at ~20 min (~20–7 kDa), representing a major portion of total Zn. This correlated with a reduction in the labile, exchangeable Zn pool appearing after 22 min in infected activated peritoneal and bone marrow macrophages (Figures 1E and 1F). Zn distribution was altered dynamically as early as 2 h and held a similar trend for the 24 h time period in infected activated peritoneal macrophages (Figures S1A and S1B).

To determine the specificity of GM-CSF in Zn modulation, macrophages were treated with the pro-inflammatory cytokine, tumor necrosis factor- α (TNF- α). TNF- α did not alter the Zn signal in macrophages (Figures 1G and 1H).

GM-CSF alters Zn transporter expression in *H. capsulatum* infected macrophages

We hypothesized that GM-CSF alters macrophage Zn distribution by regulating transporters. In an unbiased analysis of expression of Zn importers, ZIPs (*Slc39a1-14*) and exporters, ZNTs (*Slc30a1-10*), ~60 fold and 40 fold upregulation in *Slc39a2*, was observed in infected activated peritoneal and bone marrow macrophages respectively, compared to resting uninfected control (Figures 2A and 2C). A significant 2–4 fold increase in *Slc30a4* and *Slc30a7* ($p < 0.001$ for peritoneal and $p < 0.05$ for bone marrow macrophages) was also observed upon activation and infection (Figures 2B and 2D). The expression of another importer, *Slc39a8* was unchanged (Figure S2A). TNF- α treatment of did not alter *Slc39a2*, *Slc30a4* and *Slc30a7* expression (Figure 2E). These data suggest that GM-CSF activated-infected macrophages may increase Zn import and mobilize it into intracellular organelles via exporters.

Proteomics analysis of SEC fractions

GM-CSF altered the Zn-binding proteome in macrophages. For proteomics analysis, five fractions identified by SEC-ICP-MS were collected with the plasma turned-off and analyzed using a bottoms-up proteomics scheme. The list of identification parameters and proteins in all fractions and Zn-binding proteins highlighted in the fractions at ~10 and ~20 min are in

Table S1. The CCCH zinc finger protein, ZC3H12A, calreticulin and MT2 were selected as being potentially associated with immune response and Zn binding. MT2 was detected in the peak that scavenged a majority of Zn at 20 min. MT1, MT3 and ZIP2 were not identified in database search. ZIP2 is located on the cell membrane. The association of membrane proteins with hydrophobic lipids and their insolubility poses a challenge in proteomic analysis (Santoni et al., 2000). Peptide matching is compromised by complex covalent hetero-oligomerization of MT isoforms, likely explaining the absence of MT1/MT3 as hits in database search. We observed oligomerization at ~20 min based on a shift in retention time towards the high molecular weight region, with the peak showing maximal absorbance at 260 nm, typical of -S-S- bonds formed by MTs during oligomerization, and not 280 nm, representative of Trp and Tyr containing proteins (Figure S1C).

GM-CSF, but not TNF- α induces MT expression in macrophages

GM-CSF enhanced Zn binding to the ~20 min fraction in infected macrophages (Figures 1C and 1D). Proteomic analysis and UV-Vis spectral characteristics suggested a major contribution of MTs to this Zn signal (Figure S1C, S1D, and S1E). Therefore, we examined the effect of GM-CSF on *Mt* expression. GM-CSF, but not TNF- α increased *Mt1*, *Mt2* and *Mt3* expression in macrophages during infection (Figures 2F and 2G), *Mt3* is predominantly expressed in the brain (Falnoga et al., 2012). To ensure that our findings are valid, *Mt3* was examined in hepatocytes and thymocytes and was not upregulated (Figure S2B). Expression of the Zn finger ribonuclease, *Zc3h12a* was enhanced in infected macrophages but was not specific to GM-CSF (Figures S2D and S2E). GM-CSF did not alter the expression of calreticulin and of the metal response element binding transcription factor-1 (*Mtf1*) which regulates *Mt* expression (Figure S2C and S2F). Thus, GM-CSF specifically induced *Mt* expression.

GM-CSF mobilizes labile Zn away from *H. capsulatum*

Confocal microscopy was used to visualize labile Zn with the fluorescent probe, Zinpyr-1 (Cao et al., 2001). Uninfected resting peritoneal macrophages showed labile Zn distribution in the cytoplasm and epinuclear space (Figure 3A); however, Zn staining was diffuse in infected resting peritoneal macrophages (Figure 3C). GM-CSF activation caused focal Zn accumulation (Figures 3B and 3F) and mobilized Zn away from *H. capsulatum* (Figures 3D and 3G) into the Golgi apparatus (Figure 3I). The reduced Zn fluorescence of yeasts observed in GM-CSF activated macrophages was not due to an impermeability of the dye (Figure S3A). Previous reports suggest that Zinpyr-1 may localize in the Golgi (Walkup et al., 2000). To ensure that labile Zn localization was a result of cytokine stimulation, we evaluated it in TNF- α treated macrophages. Zn distribution was non-focal, no or very little Zn staining was observed in the Golgi and labile Zn was observed in yeast (Figures 3E and 3H). This is consistent with lack of changes in Zn regulation in TNF- α treated macrophages (Figures 1G, 1H, 2E and 2G). Peritoneal macrophages treated with Zn and the ionophore, pyrithione, yielded bright fluorescence and very dim staining was observed in cells treated with the Zn chelator N,N,N,N-tetrakis-(2-pyridylmethyl)-ethylenediamine (TPEN) (Figures S3B and S3C). Labile Zn was examined in alveolar macrophages, the initial phagocyte that encounters *H. capsulatum in vivo*. While staining occurred in the cytosol and Golgi in resting alveolar macrophages, GM-CSF activation caused Zn localization in the Golgi (Figures S3D-S3G). Collectively, these data suggest that GM-CSF induced Zn redistribution in macrophages, which may limit its accessibility to *H. capsulatum*.

Metallothioneins sequester and deprive *H. capsulatum* of Zn

Since Zn regulation was similar in both types of macrophages, we utilized bone marrow macrophages for further studies. To determine if Zn sequestration in macrophages and deprivation in *H. capsulatum* was caused by MTs, we took two approaches. First, we

silenced the expression of all four *Mt* genes (Figure 4A). *Mt*-silenced macrophages manifested reduced Zn binding to the chromatographic fraction at 20 min accompanied by an increase in the labile Zn fraction at ~25 min. (Figure 4B and zoom in). *H. capsulatum* recovered from *Mt* silenced macrophages had higher Zn content ($p < 0.01$) (Figure 4C). Next, we examined Zn sequestration in *Mt1^{-/-}Mt2^{-/-}* macrophages. These cells exhibited a lack of Zn-binding to the fraction at 20 min, accompanied by an increase in labile Zn in GM-CSF treated and infected macrophages (Figure 4D and zoom in). *H. capsulatum* recovered from *Mt1^{-/-}Mt2^{-/-}* macrophages had higher Zn concentration ($p < 0.01$) compared to wild type (WT) cells (Figure 4E). Thus, Zn deprivation within *H. capsulatum* resulted preponderantly from sequestration by MTs.

We queried if MT1 and MT2 participated in antimicrobial defense. We postulated that the lack of Zn sequestration in the absence of MT1 and MT2 would diminish the ability of GM-CSF to inhibit fungal growth. While *H. capsulatum* growth was inhibited in WT activated macrophages, *Mt1^{-/-}Mt2^{-/-}* activated cells showed decreased ability to limit growth of yeasts (Figure 4F).

GM-CSF engages the STAT5 and STAT3 transcriptional program to mediate Zn regulation

We sought to determine the signaling mechanism that resulted in Zn modulation. GM-CSF signals through STAT5 (Bhattacharya et al., 2001) and STAT binding sites are present on the *Mt* promoter (Lee et al., 1999). Inhibition of STAT5 and STAT3 reduced MT-Zn binding (Figure 4G and 4H). To confirm our observations with chemical inhibitors, we silenced *Stat5* and *Stat3*, which decreased Zn binding to MTs in the chromatograms of activated infected macrophages (Figures 4I, 4J and 4K).

These findings led us to postulate that GM-CSF may directly activate STAT5 and STAT3 signaling. GM-CSF increased STAT3 phosphorylation 10 min post-activation and infection, proving that the cytokine directly activated STAT3 (Figure 4L). There was >2.5 and >5 fold increase in *Mt1* and *Mt2* expression, as early as 10 min post infection and remained high for 24 h; *Mt3* was modestly altered (Figure 5A). These data indicate that Zn regulation by GM-CSF occurs via STAT5 and STAT3 signaling.

We investigated the importance of *Slc39a2* in regulating GM-CSF function. Activated infected macrophages manifested a ~10 fold increase in *Slc39a2* expression 10 min post infection (Figure 5A). We questioned whether the regulation of *Slc39a2* was a prerequisite in macrophages defense. Upregulation of *Mt* genes was partially dependent on *Slc39a2*, but silencing *Slc39a2* did not alter Zn deprivation in *H. capsulatum*, ROS production or growth inhibition (Figures 5B, 5C, S4A and S4B). *Slc39a2* silencing reduced Zn influx and MT-Zn signal in macrophages, but did not affect labile Zn sequestration (Figures 5C and 5D). To probe how MTs in these macrophages established a defensive state against the pathogen, we compared the amount of Zn bound per MT by determining the [Zn] to [S] ratio (Zn²⁺ to MTs) between control and *Slc39a2* silenced macrophages. As expected, scramble siRNA treated macrophages had increased MT and sequestered labile Zn (Figure 5D). But, the amount of Zn bound to MTs in *Slc39a2* silenced infected macrophages was ~2.4 fold greater than scramble siRNA treated control, thereby enabling efficient Zn sequestration (Figure 5E), even with lower production of MTs. Silencing *Slc39a14* did not affect GM-CSF driven macrophage defense (Figure S4C–F).

Zn sequestration enhances oxidative burst

GM-CSF enhances ROS production (Weisbart et al., 1987). Therefore, we asked if Zn sequestration affected oxidative burst during infection. GM-CSF increased ROS in macrophages. Zn chelation by TPEN in serum-free medium augmented ROS production by

~40%, which was significantly higher ($p < 0.05$) compared to activated infected macrophages (Figure 6A). This effect was reversed upon addition of $ZnSO_4$ ($p < 0.001$). To ensure that this was not due to chelation of other metals by TPEN, we specifically depleted Zn from serum-free and serum-containing media. Low-Zn serum containing media did not show a significant increase in ROS over activated infected macrophages (Figure 6A), possibly due to the presence of residual Zn contributed by serum or serum-LPS that may have an inhibitory effect on NADPH oxidase (Nox) activity. However, macrophages exposed to Zn-depleted serum-free media manifested ~36% increase in ROS, significantly higher ($p < 0.01$) than activated infected macrophages (Figure 6A). These data emphasize that a labile Zn-deprived state induced by GM-CSF facilitated increased oxidative burst, which was entirely reversible upon addition of Zn.

The sources of cellular ROS include mitochondrial respiration (Drose and Brandt, 2012) and ROS produced by Nox (Minakami and Sumimoto, 2006). Nox contributes to phagosomal ROS production that targets pathogens contained within these vacuoles. Activated macrophages from *Ncf1*^{-/-} mice failed to generate an increased ROS response upon *H. capsulatum* challenge or Zn depletion (Figure 6B), indicating that reduction in labile Zn specifically enhanced ROS generation via Nox. We postulated that ROS production would be compromised in *Mt1*^{-/-}*Mt2*^{-/-} macrophages as a consequence of reduced Zn sequestration. While WT activated infected macrophages effectively induced an oxidative burst, this was dampened in *Mt1*^{-/-}*Mt2*^{-/-} macrophages (Figure 6E).

ROS was essential for *H. capsulatum* growth inhibition; macrophages in which Nox was inhibited by apocynin and *Ncf1*^{-/-} macrophages had decreased ability to inhibit *H. capsulatum* growth (Figure 6C). To discern whether the defensive action of GM-CSF was a direct result of Zn limitation or enhanced ROS caused by Zn deprivation, we subjected *H. capsulatum* to ROS *in vitro* under Zn limitation. Though xanthine oxidase (XO) at a higher concentration reduced growth in normal media, Zn limitation greatly enhanced the inhibitory effect of ROS on *H. capsulatum* growth and this was reversible upon addition of Zn (Figure 6D). To determine the mechanism by which Zn sequestration facilitated increased Nox activity, we examined the regulation of hydrogen voltage gated proton channel (*Hvcn1*). Macrophages enhanced *Hvcn1* expression in response to GM-CSF in a STAT3 and STAT5 dependent manner (Figures 6F and S5A). Proton flux by *Hvcn1* accelerates ROS generation via Nox and Zn inhibits *Hvcn1* function (DeCoursey et al., 2003). Addition of the protonophore, carbonyl cyanide m-chlorophenyl hydrazone (CCCP) reversed the inhibitory effect of Zn on ROS generation (Figure 6G). ROS production was attenuated in *Hvcn1* silenced and *Hvcn1*^{-/-} macrophages upon GM-CSF activation and infection. *Hvcn1*^{-/-} activated macrophages showed compromised ability to control *H. capsulatum* growth compared to WT control (Figures 6G, 6H, S5B, S5C). These data signify the impact of Zn sequestration in enhancing phagocyte defense via ROS production.

GM-CSF drives Zn binding to MT *in vivo*

GM-CSF has a profound influence on the fate of infection *in vivo* (Deepe et al., 1999). We hypothesized that GM-CSF signaling was required for Zn sequestration in macrophages *in vivo*. In a pulmonary model of *H. capsulatum* infection, F4/80⁺ CD11b⁺ GFP⁺ and F4/80⁺ CD11b⁺ GFP⁻ macrophages were sorted from lung leukocytes of green fluorescent protein (GFP) *H. capsulatum* infected mice (Schematic, Figure 7A). F4/80⁺ CD11b⁺ GFP⁺ macrophages showed enhanced Zn binding to MTs compared to F4/80⁺ CD11b⁺ GFP⁻ cells (Figure 7B). To evaluate the importance of GM-CSF in Zn binding to MTs *in vivo*, it was neutralized and Zn profiles of macrophages were evaluated 7 days post infection (*p.i*). There was a sharp reduction in Zn bound to MTs in F4/80⁺ CD11b⁺ GFP⁺ macrophages in GM-CSF neutralized mice making it comparable to F4/80⁺ CD11b⁺ GFP⁻ macrophages (Figure

7D). No alteration was seen in Rat IgG controls (Figure 7C). We asked whether GM-CSF neutralization enhanced fungal burden in macrophages. The percent and MFI of GFP⁺ cells in F4/80⁺ CD11b⁺ macrophages were higher in anti-GMCSF treated mice (Figure 7F). To further examine the importance of GM-CSF signaling in Zn regulation, WT macrophages were adoptively transferred into *Csf2ra*^{-/-} mice lacking the GM-CSF receptor, infected with GFP *H. capsulatum* and WT vs. *Csf2ra*^{-/-} macrophages were sorted 7 days post infection. *Mt1*, *Mt2* and *Slc39a2* expression was enhanced in infected WT macrophages, while *Csf2ra*^{-/-} macrophages showed over 60, 93 and 97% decrease in *Mt1*, *Mt2* and *Slc39a2* expression respectively compared to infected WT macrophages (Figures 7G and 7H). Moreover, the percent infectivity of F4/80⁺ CD11b⁺ GFP⁺ cells in *Csf2ra*^{-/-} mice was higher (16.7%) as compared to infected WT CD45.1 macrophages (1.26%). These data highlight the importance of GM-CSF in regulating Zn during infection *in vivo*.

GM-CSF mediates Zn sequestration in macrophages from *Slc11a1*^{+/+} mice and from humans

C57BL/6 mice used in this study lack a functional Slc11a1 protein (White et al., 2004). This prompted us to determine if Zn regulation was altered in the presence of this Fe transporter. GM-CSF induced a similar Zn profile in macrophages from CBA/J mice that express functional Slc11a1 (Figure S6A–S6C). We asked if this phenomenon occurred in human macrophages. Zn distribution was analyzed in GM-CSF activated infected human macrophages compared with resting control. There was a similarity between Zn profiles in human and murine macrophages. Activation of human macrophages with GM-CSF elevated MT-Zn binding during infection (Figures 7E and S6G and S6H). These data indicate that GM-CSF broadly induces modulation of Zn in macrophages and that this is a conserved mechanism between mice and humans. We also determined if GM-CSF promoted Zn sequestration to a distinct clade of *H. capsulatum*, G186R. Activated macrophages strongly induced Zn modulation via MTs and Zn transporters upon infection with G186R *H. capsulatum* (Figure S6D–S6F). Thus, Zn sequestration by GM-CSF arrests pathogen survival by dually targeting fungal Zn acquisition and augmenting oxidative damage to the fungus.

DISCUSSION

This study revealed an underlying mechanism for the action of GM-CSF in combating infection with an intracellular pathogen. To date, the mechanism of GM-CSF function has not been fully elucidated. We have demonstrated that GM-CSF signaling empowers macrophage defense by facilitating a dual outcome of limitation of bioavailable Zn and simultaneous enhancement of superoxide burst which renders the pathogen susceptible to the host.

During infection, GM-CSF reduced total Zn in yeasts, but enhanced Zn influx in macrophages. Although this finding appears counterintuitive, GM-CSF induced an increase in the Zn binding proteome suggesting an enhancement of Zn dependent cellular functions such as transcription, enzyme function and metabolism (Beyersmann, 2002). To cope with pathogen invasion, activated macrophages sequestered the exchangeable Zn fraction away from intracellular fungus, while concurrently increasing ROS production.

We have reported that GM-CSF decreased total Zn in macrophages (Winters et al., 2010). The discrepancy between the current and past study is a result of an improvement in the analytical method, specifically in the blank correction of lysate analysis. We went from a flow injection analysis in a metal containing system, to a continuous flow analysis in a metal free system. The SEC-ICP-MS chromatograms manifest the same results in both studies with more total Zn in GM-CSF activated and infected peritoneal and bone marrow macrophages than the resting states by calculation of area under the curve. Also, total Zn in

H. capsulatum was consistent, since the metal free system was used in both studies. Thus, the observation that GM-CSF activation induces a state of Zn sequestration and reduces total Zn in *H. capsulatum* has been reproducibly demonstrated in this study.

Confocal microscopy revealed that GM-CSF, but not TNF- treated macrophages route labile Zn into the Golgi, in association with increased expression of *Slc30a4* and *Slc30a7* transporters that channel Zn into this organelle (Palmiter and Huang, 2004). Zn deprivation in *H. capsulatum* was unique to GM-CSF activated macrophages demonstrating the specificity of this cytokine in Zn mobilization. The Golgi acts as a site of labile Zn storage (McCormick et al., 2010), and be 'Zn-storage depot' in restricting Zn access to intracellular pathogens, while reserving it for phagocyte function. Fluorescent Zn probes are an invaluable tool in imaging Zn, but their application is affected by signal variation due to pH, ionic strength and propensity to localize in acidic compartments (Tomat and Lippard, 2010). While total cellular Zn is in micromolar range, the labile Zn pool identified using Zinpyr-1 is in the picomolar range (Eide, 2006). Hence, the observed Zn signal may represent a fraction of total Zn. Nevertheless, labile Zn is a crucial component of the total Zn pool. Immune cells deliver Zn signals upon pathogen contact and changes in labile Zn pool may reflect signal transducing properties of this metal ion (Hirano et al., 2008).

Our observations with *Mt* silenced and *Mt1^{-/-}Mt2^{-/-}* macrophages reinforce the critical function of MTs in antimicrobial defenses. In activated macrophages, MTs powered the loss of pathogen-associated Zn. We demonstrate that MTs are essential mediators of GM-CSF function and their absence presents a survival advantage to the pathogen. Of note, the WT control used in *Mt1^{-/-}Mt2^{-/-}* studies (SvJ strain) depicted a Zn regulatory response similar to C57BL/6 macrophages. Thus, interference with MT regulation impairs the antimicrobial effect induced by GM-CSF.

We showed that both STAT5 and STAT3 orchestrate Zn modulation guided by GM-CSF. Disruption of STAT5 and STAT3 signaling abrogated MT-Zn sequestration. STAT5 and STAT3 heterodimerize in the presence of granulocyte-colony stimulating factor (Novak et al., 1996); in this context, GM-CSF may also induce heterodimerization to regulate MT expression. We sought to explain Zn alteration in infected macrophages by examining transporters. ZIP2 imports Zn into the cytosol from the extracellular milieu (Eide, 2006). *Slc39a2* silencing reduced MT expression, but did not affect the ability of MTs to sequester labile Zn. Upregulation of *Slc39a2* may indicate its involvement in cellular processes that do not directly affect macrophage defense functions within the analyzed 24h period of infection. It is also plausible that the pathogen triggers Zn influx via ZIP2, an effect, counteracted by Zn sequestration in a GM-CSF primed macrophage.

Our findings reveal that Zn sequestration exerts a broader impact on macrophage antifungal defense. Conflicting evidence exists regarding the ability of Zn to trigger or dampen ROS production (Bishop et al., 2007; DeCoursey et al., 2003). In activated macrophages, a reduction in the labile Zn pool was clearly associated with an increase in ROS that was dependent on Nox and reversed by exposure to Zn. GM-CSF achieved this feat by a two-fold regulatory mechanism: first, the cytokine upregulated expression of *Hvcn1* that elevates Nox activity; second, it induced a Zn limiting environment, that promotes proton pumping by *Hvcn1* and Nox function. *Ncf1^{-/-}* and *Hvcn1^{-/-}* activated macrophages exhibited reduced growth inhibitory effect on *H. capsulatum*. Apocynin inhibits Nox, but may also interfere with NO production, and that may explain the increased reversal of inhibition (Muijsers et al., 2000). Charge compensation by K⁺ channels may account for the partial growth inhibitory capacity seen in *Hvcn1^{-/-}* activated macrophages (Nauseef, 2007). An increased ROS triggers a variety of second messenger signals, such as activation of STAT3 (Simon et al., 1998) and nuclear factor kappa B (Gloire et al., 2006) that possibly converge

into potent and sustained macrophage defense. From the pathogen perspective, Zn paucity may compromise microbial protein functions such as superoxide dismutase activity that mediates resistance to the host (Kehl-Fie et al., 2011). Metal binding sites on proteins may exhibit degeneracy (Heizmann and Cox, 1998). Zn limitation to the pathogen can therefore, potentially enforce substitution of Zn dependent metal binding sites on microbial proteins with more reactive metals, such as Cu and Fe. Indeed, the ROS generated *in vitro* by XO exerted a profound effect on *H. capsulatum* survival under Zn limitation.

Emphasizing the impact of Zn sequestration on ROS generation, we demonstrated that MTs are essential for an optimal ROS response induced by GM-CSF. In the absence of MT1 and MT2, GM-CSF failed to effectively elevate ROS. These studies were performed at an early stage, because GM-CSF triggers MTs immediately following infection. This observation is surprising, since MTs bind metals but also scavenge ROS (Maret, 2000). However, GM-CSF activated macrophages remarkably elevated Zn sequestration by MTs. The oligomeric shift in MTs may result from oxidation of Cys residues only during later stages of infection.

We have reported that lack of GM-CSF leads to detrimental fungal burden (Deepe et al., 1999). In this study, we found that blockade of GM-CSF *in vivo* was sufficient to diminish Zn sequestration and elevate macrophage fungal burden, signifying that among several cytokines, GM-CSF uniquely modulates MT-Zn homeostasis. This phenomenon may play a central role in inhibition of fungal growth *in vivo*. These mechanisms are conserved among clades of *H. capsulatum*, strains of mice and humans.

In view of diversity in defense mechanisms against distinct pathogens, human macrophages employ a unique Zn-intoxication strategy to limit growth of *M. tuberculosis*. Labile Zn deprivation by GM-CSF reveals a distinct mechanism by which the host may combat intracellular pathogens. With these contrasting mechanisms of Zn intoxication versus deprivation, it can be postulated that cytokine-activated macrophages evolved to use specialized and distinct defense arsenals against different pathogens. On the other hand, microbes have evolved means to cope with nutrient paucity. *Salmonella typhimurium* resists calprotectin mediated Zn deprivation by upregulating a high affinity Zn transporter (Liu et al., 2012). In contrast, *H. capsulatum* fails to cope with Zn sequestration and enhanced free radical challenge. Little is known about Zn transporters in *H. capsulatum*, but one may derive that, while the organism strives to acquire Zn by increasing import, the amount is insufficient to drive intracellular growth. Of note, *H. capsulatum* does not have to confront an elevated calprotectin in macrophages (Winters et al., 2010). On the other hand, it has to compete for Zn acquisition with MTs, which may be more potent than calprotectin in that each molecule of the former scavenges 7 ions with picomolar affinity (Coyle et al., 2002), while the latter binds 2 Zn ions per molecule with nanomolar affinity. (Kehl-Fie et al., 2011; Korndorfer et al., 2007).

In summary, using a combination of gene expression analysis, microscopy, ICP-MS, SEC coupled to ICP-MS and proteomics, we have dissected a mechanism by which GM-CSF activated macrophages pose a dual defense system simultaneously challenging microbial tolerance to restricted Zn availability coupled to increased oxidative damage. Lastly, we propose that labile Zn deprivation may be a global defense strategy that can be extended to growth restriction of other intracellular fungi. Whether macrophages preferentially employ labile Zn deprivation over Zn intoxication for defense against distinct microbial classes remains to be determined.

EXPERIMENTAL PROCEDURES

See also supplementary procedures.

Mice

C57BL/6, CBA/J, *Mt1^{tm1Bri}Mt2^{tm1Bri}* (*Mt1^{-/-}Mt2^{-/-}*), 129S1/SvImJ WT (control for *Mt1^{-/-}Mt2^{-/-}*) and B6.SJL-*Ptprca^a Pepcb^b*/BoyJ (CD45.1) mice were obtained from Jackson Laboratory. We thank Dr. Bruce Trapnell, Cincinnati Children's Hospital Medical Center for the *Csf2ra^{-/-}* mice; Dr. John Engelhardt, Dr. Yulong Zhang (University of Iowa), Dr. Brahm Segal, Dr. Nazmul Khan (Roswell Park Cancer Institute) and Dr. Long-Jun Wu and Dr. Jiyun Peng (Rutgers University) for providing bone marrow from *Ncf1^{-/-}* and *Hvcn1^{-/-}* mice. Animal experiments were in accordance with Animal Welfare Act guidelines of National Institutes of Health.

Activation, STAT inhibition and infection

Bone marrow macrophages were activated with cytokines for 24 h before infection. Peritoneal macrophages were rested for 24 h, followed by activation for 24 h before infection and were activated again during infection. Where indicated, macrophages were cultured throughout with 100µM STAT3 or STAT5 inhibitors, S3I-201 and N-((4-Oxo-4H-chromen-3-yl)methylene) nicotinohydrazide (Calbiochem) respectively. For infection, G217B or G186R *H. capsulatum* were cultured in Ham's F12 (Zn concentration, 250 ± 18 ng/ml or 4 µM) and washed before use.

Microscopy

Macrophages were infected with PKH-26 stained *H. capsulatum* for 24 h followed by staining with nuclear, Golgi and Zn dyes where indicated for 30 min. Images were acquired on a Zeiss LSM710 confocal and analyzed using ZEN 2011 software.

Silencing

Genes were silenced using TransIT-TKO transfection reagent (Mirus Bio LLC) and 100nM Mt (Santa Cruz), Slc39a2, Slc39a14, Stat3 or Stat5 (50nM each of Stat5a and Stat5b), Hvcn1 or scrambled siRNA (Dharmacon) as per manufacturer's instructions.

ROS

Macrophages were activated for 24h and then incubated with 5µM Dihydroethidium (DHE) (Invitrogen) in fresh media for 15 min in dark, followed by GM-CSF and infected for 2h. Where indicated, 100µM ZnSO₄ and TPEN or Zn depleted media was added 20 min prior to DHE. CCCP was added 30 min before analysis by flow cytometry (Accuri C6). Data were analyzed with FCS Express 3 De Novo Software (CA) or FlowJo.

In vivo

Eight week old C57BL/6 mice were infected with 2×10^6 GFP⁺ *H. capsulatum* yeasts *i.n.* Mice were injected ip. with 0.5mg control mAb Rat IgG2a (BioXcell) or MP1-22E9 mAb Rat IgG2a anti-GM-CSF a day before and on the day of infection. After 7 days, lungs were homogenized with gentleMACS Dissociator (Miltenyi Biotec, CA), collagenase treated, filtered through 60 µM nylon mesh and washed. Leukocytes were isolated using Lympholyte M (Cedarlane Laboratories, Canada) and stained with APC F4/80 (AbD Serotec) and PerCP CD11b mAbs (BD Biosciences) and CD16/CD32 blocking mAbs for 30 min at 4°C and washed; gated on F4/80⁺CD11b⁺ and sorted into GFP⁺ (containing phagocytosed *H. capsulatum*) and GFP⁻ (not containing *H. capsulatum*) using 5-laser FACS Aria II (BD Biosciences) in a BSLII facility at Cincinnati Children's Hospital; collected at 4°C in culture media and washed prior to lysis. For adoptive transfer, 2×10^6 bone marrow macrophages from WT (CD45.1) were transferred intratracheally into 8 week old *Csfr2a^{-/-}* (CD45.2) mice 1 day prior to *H. capsulatum* infection. On day 7 post infection, lung

leukocytes were sorted into 4 populations: F4/80⁺CD11b⁺CD45.1⁺GFP⁻ or GFP⁺ and F4/80⁺CD11b⁺CD45.1⁻GFP⁻ or GFP⁺ macrophages for analysis of gene expression.

Human macrophages

PBMCs were isolated from human blood (Hoxworth Blood Center, University of Cincinnati) using Ficoll-Paque. Monocytes were purified with Monocyte Isolation Kit II on a VarioMACS separator (Miltenyi Biotec) and cultured in RPMI with 12.5% human male AB serum (Sigma-Aldrich) for 7 days, and macrophages were exposed to 10 ng/ml GM-CSF (Peprotech) or vehicle for 24 h before infection, re-exposed to GM-CSF at the time of infection and lysates were prepared 24 h later.

Cell lysates for ICP-MS

Macrophages were washed and lysed with 0.1% sodium dodecyl sulfate (SDS) in HPLC water for 20 min on ice. Lysates were passed through a 0.22 μ m filter or centrifuged at 13,000rpm for 5 min for analysis. For total metal analysis of *H. capsulatum*, lysates were centrifuged at 13,000rpm for 5 min to pellet the yeasts and the pellet was washed twice with HBSS.

Total elemental analysis and SEC-ICP-MS screening

ICP-MS analysis was performed on Agilent 7700x ICP-MS instrument (Agilent Technologies). A conventional Meinhard nebulizer, Peltier-cooled spray chamber, and shield torch constituted the sample introduction system under standard conditions. Sc was used as internal standard and SRM (DORM-3 or NIST1745) were analyzed for every digestion.

For SEC-ICP-MS, Agilent 1100 series HPLC system equipped with a binary pump, vacuum membrane degasser, thermostated auto sampler, column oven, and diode array detector (DAD), with a semi-micro flow UV-Vis cell was coupled to the ICP-MS through a 0.17mm internal diameter short PEEK tube. The system was controlled with Chemstation software. A TSK Gel 3000SW 7.5 \times 300 mm column was used. For proteomics, samples were concentrated before injection using MWCO filter 3 kDa (Millipore). For analysis of MT saturation, the MTs-SEC signal (20 min) was collected and analyzed for S and Zn to determine the MT:Zn ratio in a Superdex peptide SEC-ICP-MS using O₂ reaction mode.

Proteomics

The SEC-ICP-MS fractions were analyzed using an Agilent 1200 nanoHPLC, nanoChip ESI and 6300 series MSD Ion Trap XCT Ultra system. Peptide and corresponding protein identification were conducted using MASCOT server (Matrix Science).

Statistics

p-values were calculated using one way ANOVA for multiple comparisons and adjusted with Bonferroni's or Holm Sidak correction; and non-paired Student *t* test where two groups were compared; *p<0.05; **p<0.01; ###p<0.001; NS, not significant.

Supplementary Material

Refer to Web version on PubMed Central for supplementary material.

Acknowledgments

We thank Agilent Technologies for instrumentation, ICP-MS and nanoHPLC-ESI-IT-MS and Drs. B. Klein, W. Nauseef, and D. Hildeman for their valuable feedback. This work was supported by grants from the NIH, AI-094971, AI-106269 and a Merit Review from Veterans Affairs.

References

- Appelberg R. Macrophage nutriprive antimicrobial mechanisms. *J Leukoc Biol.* 2006; 79:1117–1128. [PubMed: 16603587]
- Beyersmann D. Homeostasis and cellular functions of zinc. *Materialwissenschaft und Werkstofftechnik.* 2002; 33:764–769.
- Bhattacharya S, Stout BA, Bates ME, Bertics PJ, Malter JS. Granulocyte macrophage colony-stimulating factor and interleukin-5 activate STAT5 and induce CIS1 mRNA in human peripheral blood eosinophils. *American Journal of Respiratory Cell and Molecular Biology.* 2001; 24:312–316. [PubMed: 11245630]
- Bishop GM, Dringen R, Robinson SR. Zinc stimulates the production of toxic reactive oxygen species (ROS) and inhibits glutathione reductase in astrocytes. *Free Radic Biol Med.* 2007; 42:1222–1230. [PubMed: 17382203]
- Botella H, Peyron P, Levillain F, Poincloux R, Poquet Y, Brandli I, Wang C, Tailleux L, Tilleul S, Charriere GM, et al. Mycobacterial p(1)-type ATPases mediate resistance to zinc poisoning in human macrophages. *Cell Host Microbe.* 2011; 10:248–259. [PubMed: 21925112]
- Cao J, Bobo JA, Liuzzi JP, Cousins RJ. Effects of intracellular zinc depletion on metallothionein and ZIP2 transporter expression and apoptosis. *J Leukoc Biol.* 2001; 70:559–566. [PubMed: 11590192]
- Coyle P, Philcox JC, Carey LC, Rofe AM. Metallothionein: the multipurpose protein. *Cell Mol Life Sci.* 2002; 59:627–647. [PubMed: 12022471]
- DeCoursey TE, Morgan D, Cherny VV. The voltage dependence of NADPH oxidase reveals why phagocytes need proton channels. *Nature.* 2003; 422:531–534. [PubMed: 12673252]
- Deepe GS Jr, Gibbons R, Woodward E. Neutralization of endogenous granulocyte-macrophage colony-stimulating factor subverts the protective immune response to *Histoplasma capsulatum*. *J Immunol.* 1999; 163:4985–4993. [PubMed: 10528203]
- Drose S, Brandt U. Molecular mechanisms of superoxide production by the mitochondrial respiratory chain. *Adv Exp Med Biol.* 2012; 748:145–169. [PubMed: 22729857]
- Eide DJ. Zinc transporters and the cellular trafficking of zinc. *Biochim Biophys Acta.* 2006; 1763:711–722. [PubMed: 16675045]
- Falnoga I, Zelenik Pevec A, Slejkovec Z, Znidaric MT, Zajc I, Mlakar SJ, Marc J. Arsenic Trioxide (ATO) Influences the gene expression of metallothioneins in human glioblastoma cells. *Biol Trace Elem Res.* 2012
- Fang FC. Perspectives series: host/pathogen interactions. mechanisms of nitric oxide-related antimicrobial activity. *J Clin Invest.* 1997; 99:2818–2825. [PubMed: 9185502]
- Fraker PJ, Gershwin ME, Good RA, Prasad A. Interrelationships between zinc and immune function. *Fed Proc.* 1986; 45:1474–1479. [PubMed: 3485544]
- Gloire G, Legrand-Poels S, Piette J. NF-kappaB activation by reactive oxygen species: fifteen years later. *Biochem Pharmacol.* 2006; 72:1493–1505. [PubMed: 16723122]
- Heizmann CW, Cox JA. New perspectives on S100 proteins: a multi-functional Ca²⁺-, Zn²⁺- and Cu²⁺-binding protein family. *BioMetals.* 1998; 11:383–397. [PubMed: 10191501]
- Hirano T, Murakami M, Fukada T, Nishida K, Yamasaki S, Suzuki T. Roles of zinc and zinc signaling in immunity: zinc as an intracellular signaling molecule. *Adv Immunol.* 2008; 97:149–176. [PubMed: 18501770]
- Howard DH. Intracellular behavior of *Histoplasma capsulatum*. *J Bacteriol.* 1964; 87:33–38. [PubMed: 14102870]
- Kauppinen TM, Higashi Y, Suh SW, Escartin C, Nagasawa K, Swanson RA. Zinc triggers microglial activation. *J Neurosci.* 2008; 28:5827–5835. [PubMed: 18509044]

- Kehl-Fie, Thomas E.; Chitayat, S.; Hood, MI.; Damo, S.; Restrepo, N.; Garcia, C.; Munro, Kim A.; Chazin, Walter J.; Skaar, Eric P. Nutrient Metal Sequestration by Calprotectin Inhibits Bacterial Superoxide Defense, Enhancing Neutrophil Killing of *Staphylococcus aureus*. *Cell Host & Microbe*. 2011; 10:158–164. [PubMed: 21843872]
- Kitamura H, Morikawa H, Kamon H, Iguchi M, Hojyo S, Fukada T, Yamashita S, Kaisho T, Akira S, Murakami M, Hirano T. Toll-like receptor-mediated regulation of zinc homeostasis influences dendritic cell function. *Nat Immunol*. 2006; 7:971–977. [PubMed: 16892068]
- Korndorfer IP, Brueckner F, Skerra A. The crystal structure of the human (S100A8/S100A9)₂ heterotetramer, calprotectin, illustrates how conformational changes of interacting alpha-helices can determine specific association of two EF-hand proteins. *J Mol Biol*. 2007; 370:887–898. [PubMed: 17553524]
- Lee DK, Carrasco J, Hidalgo J, Andrews GK. Identification of a signal transducer and activator of transcription (STAT) binding site in the mouse metallothionein-I promoter involved in interleukin-6-induced gene expression. *Biochem J*. 1999; 337(Pt 1):59–65. [PubMed: 9854025]
- Liu JZ, Jellbauer S, Poe AJ, Ton V, Pesciaroli M, Kehl-Fie TE, Restrepo NA, Hosking MP, Edwards RA, Battistoni A, et al. Zinc sequestration by the neutrophil protein calprotectin enhances *Salmonella* growth in the inflamed gut. *Cell Host Microbe*. 2012; 11:227–239. [PubMed: 22423963]
- Maret W. The Function of Zinc Metallothionein: A Link between Cellular Zinc and Redox State. *The Journal of Nutrition*. 2000; 130:1455S–1458S. [PubMed: 10801959]
- McCormick N, Velasquez V, Finney L, Vogt S, Kelleher SL. X-ray fluorescence microscopy reveals accumulation and secretion of discrete intracellular zinc pools in the lactating mouse mammary gland. *PLoS One*. 2010; 5:e11078. [PubMed: 20552032]
- McDevitt CA, Ogunniyi AD, Valkov E, Lawrence MC, Kobe B, McEwan AG, Paton JC. A molecular mechanism for bacterial susceptibility to zinc. *PLoS Pathog*. 2011; 7:e1002357. [PubMed: 22072971]
- Minakami R, Sumimoto H. Phagocytosis-coupled activation of the superoxide-producing phagocyte oxidase, a member of the NADPH oxidase (nox) family. *Int J Hematol*. 2006; 84:193–198. [PubMed: 17050190]
- Mosser DM. The many faces of macrophage activation. *J Leukoc Biol*. 2003; 73:209–212. [PubMed: 12554797]
- Muijsers RB, van Den Worm E, Folkerts G, Beukelman CJ, Koster AS, Postma DS, Nijkamp FP. Apocynin inhibits peroxynitrite formation by murine macrophages. *Br J Pharmacol*. 2000; 130:932–936. [PubMed: 10864902]
- Nairz M, Fritsche G, Brunner P, Talasz H, Hantke K, Weiss G. Interferon-gamma limits the availability of iron for intramacrophage *Salmonella typhimurium*. *Eur J Immunol*. 2008; 38:1923–1936. [PubMed: 18581323]
- Nauseef WM. How human neutrophils kill and degrade microbes: an integrated view. *Immunol Rev*. 2007; 219:88–102. [PubMed: 17850484]
- Newman SL, Gootee L. Colony-stimulating factors activate human macrophages to inhibit intracellular growth of *Histoplasma capsulatum* yeasts. *Infect Immun*. 1992; 60:4593–4597. [PubMed: 1398972]
- Novak U, Mui A, Miyajima A, Paradiso L. Formation of STAT5-containing DNA binding complexes in response to colony-stimulating factor-1 and platelet-derived growth factor. *J Biol Chem*. 1996; 271:18350–18354. [PubMed: 8702476]
- Palmeter RD, Huang L. Efflux and compartmentalization of zinc by members of the SLC30 family of solute carriers. *Pflugers Arch*. 2004; 447:744–751. [PubMed: 12748859]
- Santoni V, Molloy M, Rabilloud T. Membrane proteins and proteomics: un amour impossible? *Electrophoresis*. 2000; 21:1054–1070. [PubMed: 10786880]
- Simon AR, Rai U, Fanburg BL, Cochran BH. Activation of the JAK-STAT pathway by reactive oxygen species. *Am J Physiol*. 1998; 275:C1640–1652. [PubMed: 9843726]
- Tomat E, Lippard SJ. Imaging mobile zinc in biology. *Curr Opin Chem Biol*. 2010; 14:225–230. [PubMed: 20097117]

- Walkup GK, Burdette SC, Lippard SJ, Tsien RY. A new cell-permeable fluorescent probe for Zn²⁺ J Am Chem Soc. 2000;122.
- Weisbart RH, Kwan L, Golde DW, Gasson JC. Human GM-CSF primes neutrophils for enhanced oxidative metabolism in response to the major physiological chemoattractants. Blood. 1987; 69:18–21. [PubMed: 3024757]
- White JK, Stewart A, Popoff JF, Wilson S, Blackwell JM. Incomplete glycosylation and defective intracellular targeting of mutant solute carrier family 11 member 1 (Slc11a1). Biochem J. 2004; 382:811–819. [PubMed: 15202932]
- Winters MS, Chan Q, Caruso JA, Deepe GS Jr. Metallomic analysis of macrophages infected with *Histoplasma capsulatum* reveals a fundamental role for zinc in host defenses. J Infect Dis. 2010; 202:1136–1145. [PubMed: 20731582]
- Zwilling BS, Kuhn DE, Wikoff L, Brown D, Lafuse W. Role of iron in Nramp1-mediated inhibition of mycobacterial growth. Infect Immun. 1999; 67:1386–1392. [PubMed: 10024586]

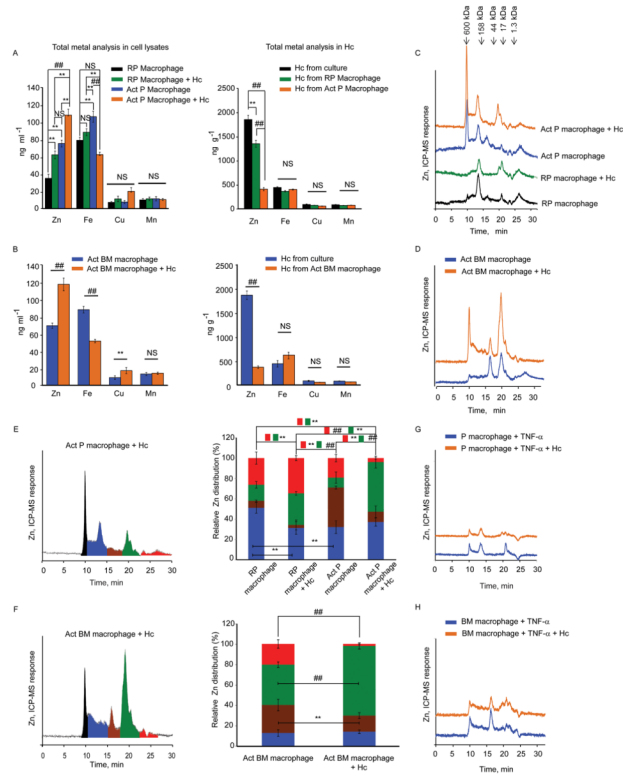


Figure 1. GM-CSF distinctly modulates Zn-distribution in infected macrophages

Total concentration of Zn by ICP-MS in (A, B) lysates from peritoneal and bone marrow macrophages; RP, resting peritoneal, Act, GM-CSF activated, and, total Zn analysis by ICP-MS in *H. capsulatum* (Hc) recovered from macrophages and compared with yeasts grown in Ham's F12 media, data are mean \pm SD, 4 independent experiments. The cell lysate concentrations are based on 2.5×10^6 cells in $\sim 200 \mu\text{l}$; *H. capsulatum* concentration was calculated based on mass of yeasts recovered; (C, D) typical SEC-ICP-MS chromatograms of activated peritoneal and bone marrow macrophages, compared to resting conditions; (E, F) Left panel, Graphical representation of color coded peaks depicting Zn distribution in various MW fractions in the chromatograms of infected activated peritoneal and bone marrow macrophages; middle panel, Zn distribution calculated as area under the curve of individual peaks against the total area; red and green boxes with **, ## symbol indicate significant differences in the corresponding color coded fractions between different groups; data are mean \pm SD, 4 independent experiments; (G, H) Typical SEC-ICP-MS chromatograms of TNF- α treated macrophages, 3 independent experiments, Y axis in all chromatograms is off-set to allow easy comparison under the same scale. Related to Figure S1 and Table S1.

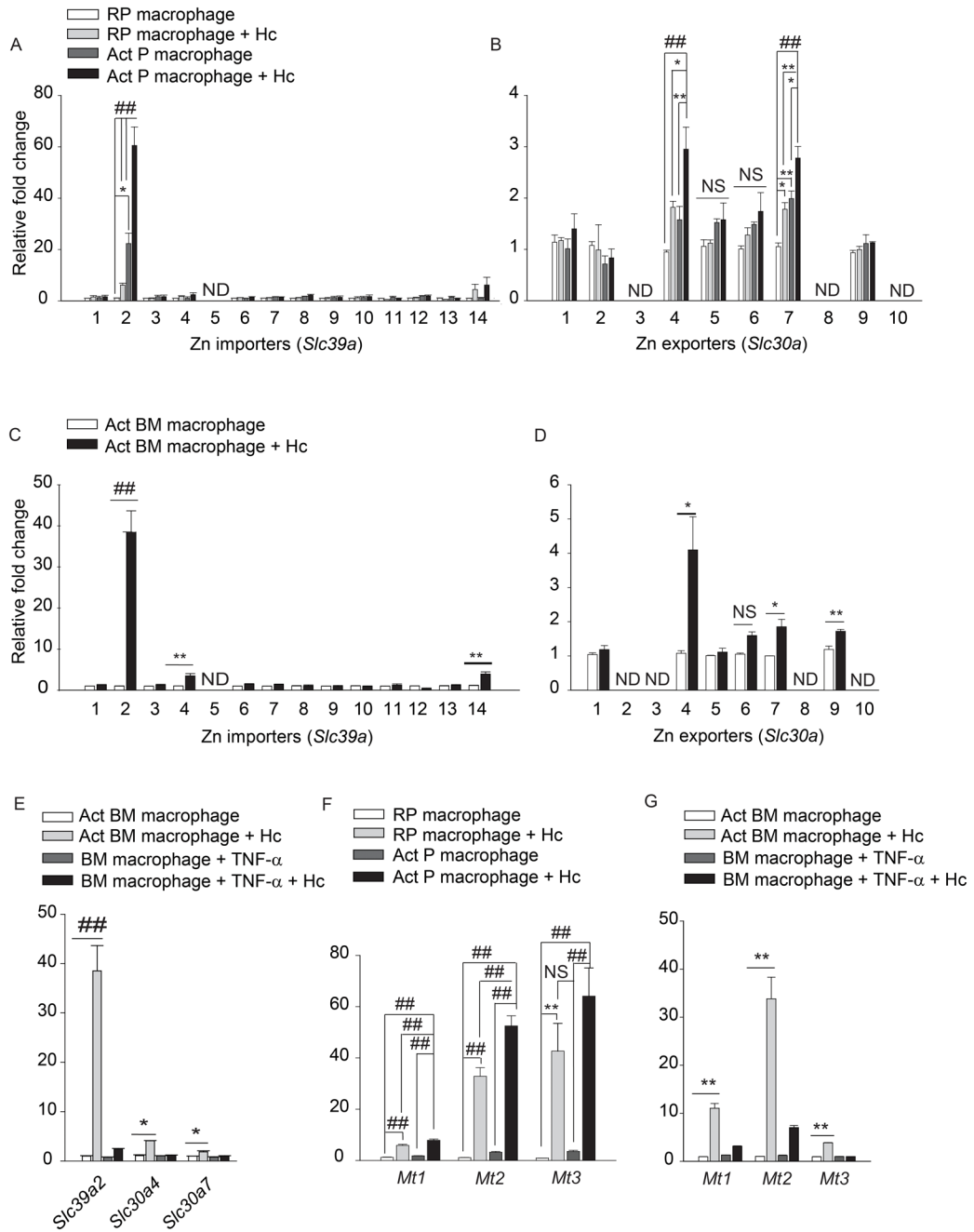


Figure 2. GM-CSF alters Zn transporter and MT expression
 qRT-PCR of *Slc39a* and *Slc30a* in (A, B) peritoneal; (C, D) bone marrow; (E) TNF- α treated macrophages, data are mean \pm SEM, 3 independent experiments; (F, G) *Mt1*, *Mt2* and *Mt3* expression in macrophages; RP, resting peritoneal; Act, GM-CSF activated; Hc, *H. capsulatum*, data are mean \pm SEM, 8 independent experiments; ND, not detected. Related to Figure S2.

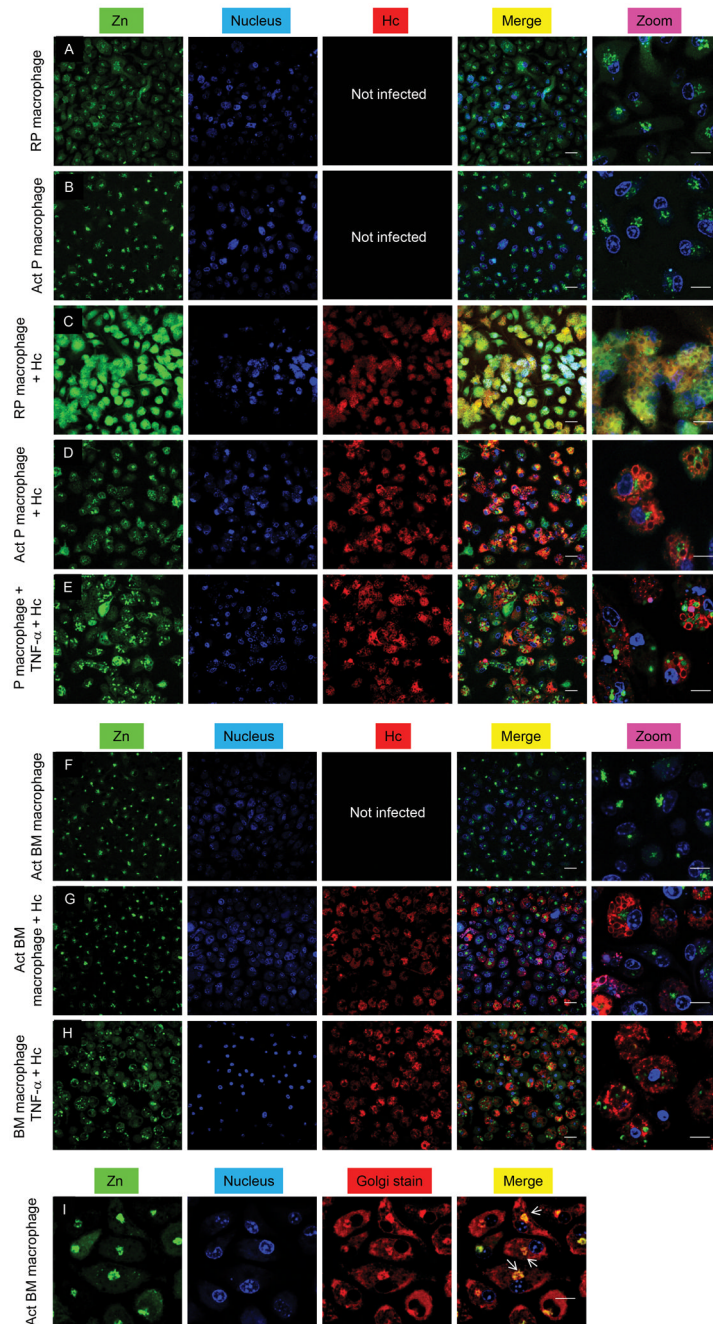


Figure 3. GM-CSF, but not TNF- α triggers Zn mobilization

Confocal microscopic analysis of Zn (green), nucleus (blue) and *H. capsulatum* (Hc) (red) in (A–E) peritoneal; (F–H) bone marrow macrophages; merge, overlay of Zn, nucleus and *H. capsulatum*; (I) Staining for Zn (green), nucleus (blue) and Golgi (red); merge, overlay of Zn, nucleus and Golgi; yellow, co-localization of Golgi and Zn dyes; white arrows point at the Golgi; scale bars, 20 μ m; RP, resting peritoneal; Act, activated; 3 independent experiments. Related to Figure S3.

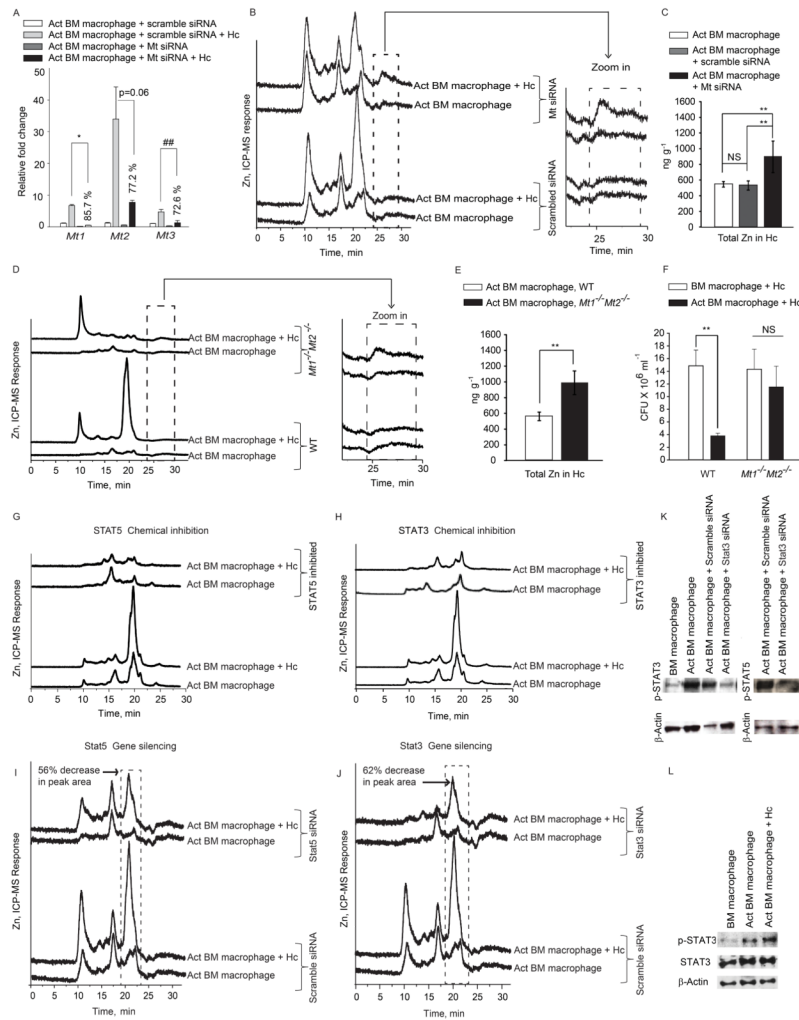


Figure 4. GM-CSF engages the STAT5 and STAT3 transcriptional program to regulate MT-Zn sequestration

(A) qRT-PCR of *Mt* genes in activated (Act) macrophages treated with scramble or *Mt* siRNA, % decrease in expression compared to scramble siRNA control, data are mean \pm SEM, 2 independent experiments; (B, D) SEC-ICP-MS chromatograms of *Mt* silenced activated infected (Hc) macrophages and from WT and *Mt1*^{-/-}*Mt2*^{-/-} mice and zoom in of labile Zn fraction, 2 independent experiments; (C, E) Total metal analysis of Zn in *H. capsulatum* (Hc) from *Mt* silenced and WT, *Mt1*^{-/-}*Mt2*^{-/-} macrophages, data are mean \pm SD, 2 independent experiments; (F) Colony forming units (CFU) of *H. capsulatum* 24 h post infection from WT and *Mt1*^{-/-}*Mt2*^{-/-} activated macrophages compared to untreated control; data are mean \pm SEM, 4 independent experiments; (G–J) SEC-ICP-MS chromatograms of chemically inhibited and *Stat3* and *Stat5* silenced macrophages, % decrease in peak area is compared to scramble siRNA treated infected macrophages; Y axis, Offset Zn-signal, 3 independent experiments; (K) p-STAT3, p-STAT5 and -actin from silenced macrophages 24 h post activation, n=2; (L) Western blot of p-STAT3, STAT3 and -actin from lysates 10 min post activation and infection, n=2.

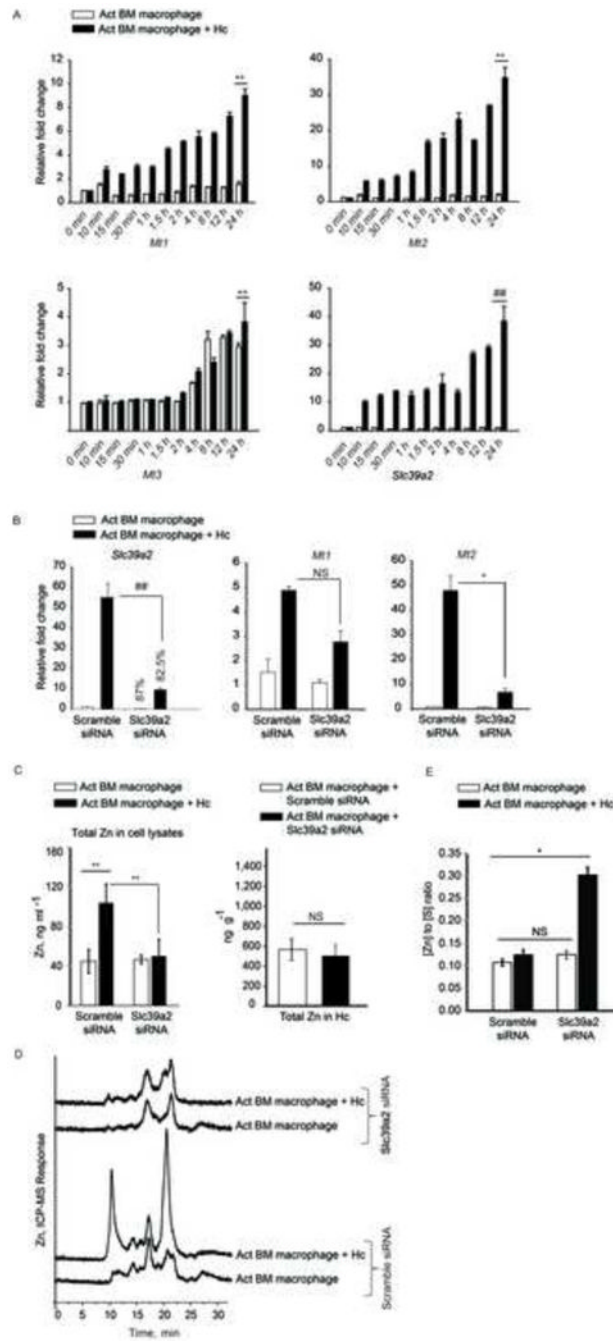


Figure 5. Early regulation of *Mt* genes and role of *Slc39a2* in MT-Zn sequestration

(A) qRT-PCR of *Mt1*, *Mt2*, *Mt3* and *Slc39a2*, time points are min and h post infection, data are mean \pm SEM, n=3 at 0–12 h and n=10 independent experiments at 24 h; (B) qRT-PCR of *Slc39a2*, *Mt1* and *Mt2* in *Slc39a2* silenced macrophages normalized to scramble siRNA control, % decrease in expression compared to respective scramble controls, data are mean \pm SEM, 3 independent experiments; (C) Total metal analysis of Zn in lysates (left) and *H. capsulatum* (right) from scramble siRNA and *Slc39a2* silenced macrophages, data are mean \pm SD, 3 independent experiments; (D) SEC-ICP-MS chromatogram of scramble siRNA and *Slc39a2* silenced activated macrophages, Y axis, Offset Zn- signal; right panel, zoom in of labile Zn fraction, 3 independent experiments; (E) Ratio of Zn to sulfur in the MT fraction

collected from 19 to 21 min based on the areas under the chromatogram corrected by differences in sensitivity through calibration with S and Zn standards, data are mean \pm SD, 3 independent experiments. Related to Figure S4.

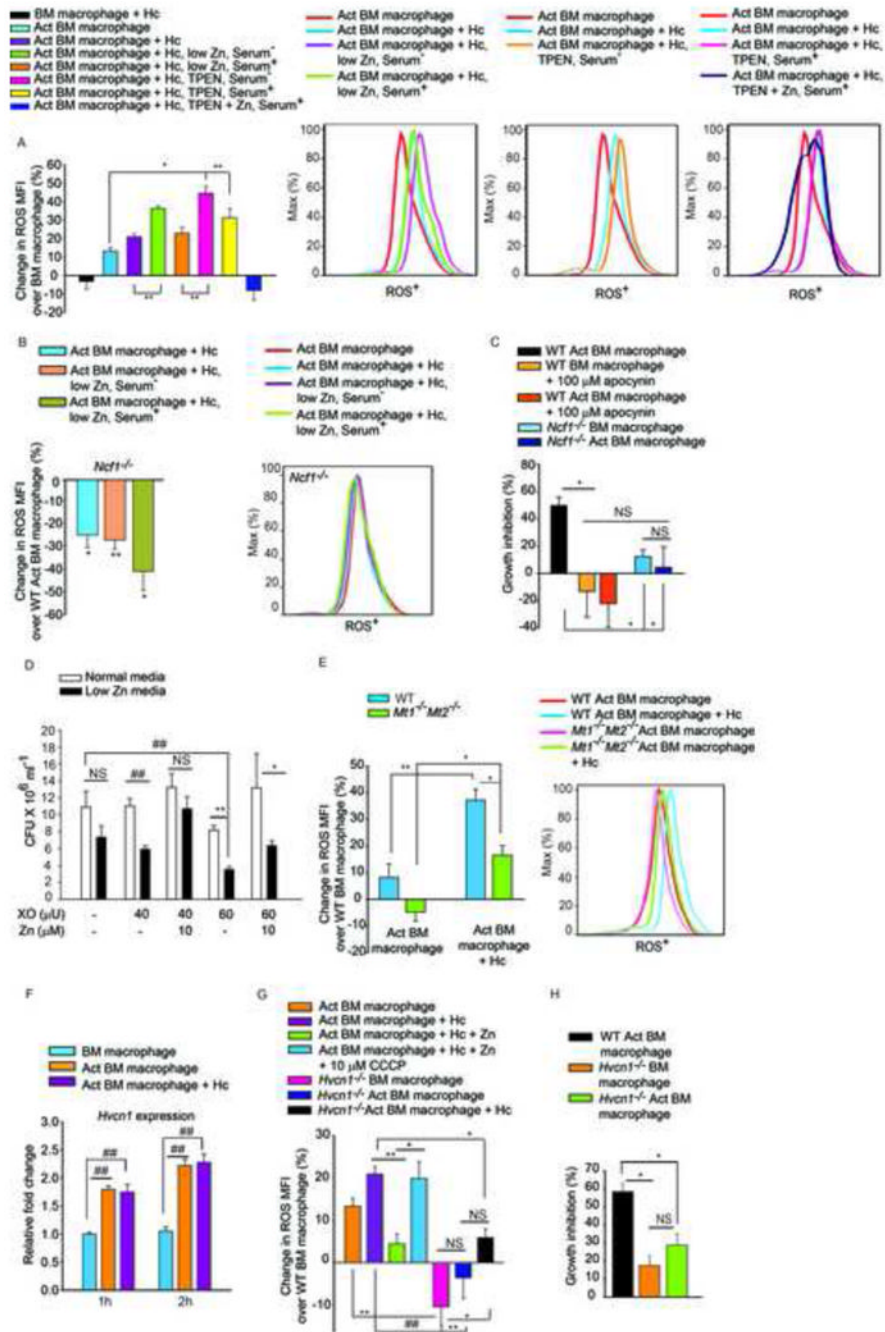


Figure 6. Zn sequestration enhances ROS production

(A) % Change in ROS MFI in cells cultured in Zn replete, low Zn serum⁻, low Zn serum⁺, 10 μM TPEN serum⁻, 20 μM TPEN serum⁺, and 20 μM TPEN with 100 μM ZnSO₄ treated serum⁺ media, serum⁻ media was included as serum containing media has considerably higher Zn. Where serum⁺ media was used, a higher concentration of TPEN was added (20μM), last group is significantly different (p<0.01) from all groups; ROS histograms demonstrating the effect of Zn sequestration; Act, activated, Hc, *H. capsulatum*, 2–3 independent experiments; (B) % change in ROS MFI in *Ncf1*^{-/-} activated macrophages, compared to WT activated uninfected cells, 3 independent experiments, histogram from *Ncf1*^{-/-} macrophages; (C) % inhibition of yeast growth in apocynin treated or *Ncf1*^{-/-}

activated over WT macrophages, 3 independent experiments; **(D)** CFU of *H. capsulatum* in normal or low Zn media with increasing concentration of XO, with or without addition of Zn, 3 independent experiments; **(E)** % change in ROS MFI in WT and *Mt1^{-/-}Mt2^{-/-}* macrophages compared to WT uninfected cells, ROS histogram of WT and *Mt1^{-/-}Mt2^{-/-}* macrophages, 3 independent experiments; **(F)** *Hvcn1* expression normalized to untreated macrophages, 3 independent experiments; **(G)** % change in ROS MFI in WT activated macrophages in response to infection, Zn and CCCP, 2 independent experiments, and *Hvcn1^{-/-}* activated cells compared to WT, 3 independent experiments; **(H)** % inhibition of *H. capsulatum* growth in infected and activated WT vs *Hvcn1^{-/-}* macrophages over WT control, 3 independent experiments; all data are mean \pm SEM. Related to Figure S5.

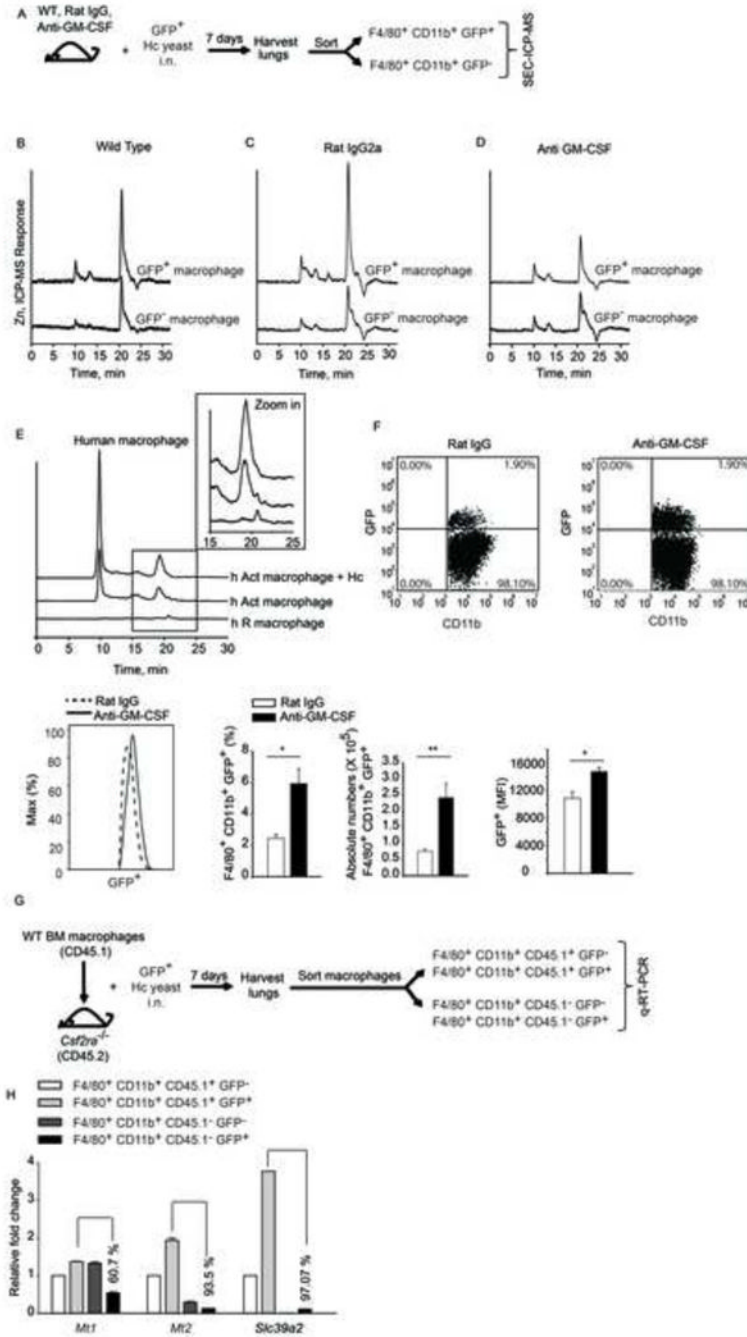


Figure 7. GM-CSF triggers Zn binding to MTs *in vivo* and in human macrophages
(A) Schematic, mice were left untreated or treated with rat IgG or anti-GM-CSF and infected *i.n.* with 2×10^6 GFP⁺ yeasts (Hc); lungs were harvested 7 days *p.i.* and F4/80⁺CD11b⁺GFP⁺ and F4/80⁺CD11b⁺GFP⁻ cells were sorted. SEC-ICP-MS profiles of **(B)** F4/80⁺CD11b⁺GFP⁺ and F4/80⁺ CD11b⁺GFP⁻ cells isolated from lungs; **(C)** rat IgG treated and **(D)** anti-GM-CSF treated mice, 2 independent experiments; **(E)** SEC-ICP-MS profiles of lysates from human resting (h R) and GM-CSF activated (h Act) macrophages; Y axis, offset Zn signal; inset, *zoom in* of 15–25 min fraction, 2 independent experiments; **(F)** Dot plot of lung leukocytes gated on F4/80⁺CD11b⁺ macrophages; histogram of F4/80⁺CD11b⁺GFP⁺ macrophages; bar graphs are quantification of %, absolute numbers

and MFI of F4/80⁺CD11b⁺GFP⁺ macrophages in rat IgG vs anti-GM-CSF treated mice, data are mean \pm SEM, n=4; **(G)** Schematic representing transfer of CD45.1 WT macrophages into CD45.2 *Csf2ra*^{-/-} mice, infection and sorting of WT vs *Csf2ra*^{-/-} macrophages from lungs for gene expression analysis; **(H)** qRT-PCR of *Mt1*, *Mt2* and *Slc39a2* from sorted CD45.1⁺ (WT) and CD45.1⁻ (*Csf2ra*^{-/-}) GFP⁻ and GFP⁺ macrophages normalized to CD45.1⁺GFP⁻ macrophages, % values are decrease in gene expression in *Csf2ra*^{-/-} CD45.1⁻ GFP⁺ macrophages compared to WT CD45.1⁺ GFP⁺ macrophages, data are mean \pm SEM, data are from 1 experiment. Related to Figure S6.